ACS APPLIED MATERIALS & INTERFACES

Research Article

www.acsami.org

Exploring the Heterogeneous Interfaces in Organic or Ruthenium Dye-Sensitized Liquid- and Solid-State Solar Cells

Young Soo Kwon, Inwoo Song, Jong Chul Lim, In Young Song, Ayyanar Siva, and Taiho Park*

Department of Chemical Engineering, Pohang University of Science and Technology, San 31, Hyoja-dong, Nam-gu, Pohang, Gyungbuk, Korea

ABSTRACT: The interfacial properties were systematically investigated using an organic sensitizer (3-(5′-{4-[(4-*tert*-butyl-phenyl)-*p*-tolyl-amino]-phenyl}-[2,2′]bithiophenyl-5-yl)-2-cyano-acrylic acid (**D**)) and inorganic sensitizer (bis(tetrabutylammonium) cis-bis-(thiocyanato)bis(2,2′-bipyridine-4,4′-dicarboxylato) ruthenium(II) (**N719**)) in a liquid-state and a solid-state dye-sensitized solar cell (DSC). For liquid-DSCs, the faster charge recombination for the surface of **D**-sensitized TiO_2 resulted in shorter diffusion length (L_D) of ~3.9 μm than that of **N719** (~7.5 μm), limiting the solar cell performance at thicker films used in liquid-DSCs. On the other hand, for solid-DSCs using thin TiO_2 films (~ 2 μm), **D**-sensitized device outperforms the **N719**-sensitized device in an identical fabrication condition, mainly due to less perfect wetting ability of solid hole conductor into the porous TiO_2 network, inducing the dye monolayer act as an insulation layer, while liquid electrolyte is able to fully wet the surface of TiO_2. Such insulation effect was attributed to the fact that the significant increase in recombination resistance (from 865 to 4,400 Ω/cm^2) but shorter electron lifetime (from 10.8 to 0.8 ms) when compared to liquid-DSCs. Higher recombination resistance for solid-DSCs induced the electron transport-limited situation, showing poor performance of **N719**-sensitized device which has shorter electron transport time and similar L_D (2.9 μm) with **D**-sensitized device (3.0 μm).

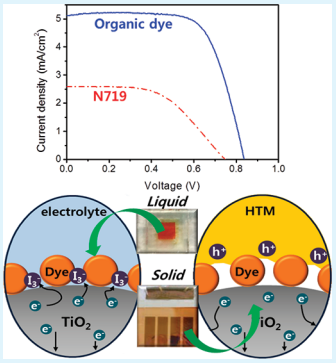

KEYWORDS: *dye-sensitized solar cells, organic dye, solid-state, light harvesting, recombination*

INTRODUCTION

Since Grätzel's first demonstration of dye-sensitized solar cells (DSCs) in 1991,[1] DSCs have been extensively studied in an effort to exploit their high power conversion efficiency and low production costs.[2−7] The maximum efficiency of liquid electrolyte-based DSCs currently exceeds 11%.[8,9] Whereas ruthenium(II) polypyridyl complexes and their analogues perform remarkably well in DSCs, metal-free organic dyes are promising alternatives to ruthenium complexes owing to high molar extinction coefficients, tunable optical and electrochemical properties, and low costs.[10] Numerous organic dyes have been studied for use in DSCs,[11] including perylene derivatives,[12,13] coumarin dyes,[14,15] porphyrin dyes,[16] cyanine dyes,[17] and indoline dyes,[18,19] and the efficiencies of such DSCs exceed 9%. Thin TiO_2 films are optimal for taking advantage of their unique optical properties in the visible region, which is particularly important for iodine-free solid- DSCs that incorporate solid hole transporting materials (HTMs)[20−22] in which an optimized TiO_2 layer thickness of 2−3 μm provides efficient charge collection.[23] State-of-the-art solid-DSCs that incorporate organic dyes have yielded efficiencies exceeding 6%.[24,25]

The outstanding performance of organic dye-containing solid-DSCs is derived from a good light harvesting efficiency (LHE) in thin films rather than from the interfacial properties of the TiO_2/dye/electrolyte (the HTM). However, DSC performance is sensitive to the heterojunction interface at which photoinduced charge transfer processes take place.[26,27] For instance, the relative energy levels of the dye, electrolyte (the HTM), and additives at the interface influence the solar cell performance by altering the electron injection and dye regeneration processes.[6] Furthermore, charge recombination between photoinjected electrons and oxidized species in the electrolyte or HTM contribute to loss, which limits the short circuit current (I_{SC}) and open circuit voltage (V_{OC}).

In considering whether to exploit the properties of organic dyes in DSCs, the light harvesting and interfacial properties must be compared with those of ruthenium complexes in liquid- and solid-DSCs. Miyashita et al. investigated electron-transfer kinetics of organic dye-sensitized solar cells compared with ruthenium complexes depending on the dye structure and electrolytes.[28] They revealed lower V_{OC} for organic DSCs originated from short electron lifetime than that of ruthenium-DSCs. Cai et al. recently reported organic dye-sensitized solid-state solar cells in which the organic dye C220 outperformed the ruthenium dye Z907 because of its longer electron lifetime and higher charge collection efficiency.[25] These studies compared organic dyes with ruthenium dyes in a single type of system, or organic dyes were tested alone in liquid- or solid-DSCs.

Here, we compared the performance of organic dyes in liquid- and solid-DSCs to ruthenium complexes in an effort to

Received: March 18, 2012
Accepted: June 1, 2012
Published: June 1, 2012

   dx.doi.org/10.1021/am300480j | *ACS Appl. Mater. Interfaces* 2012, 4, 3141−3147

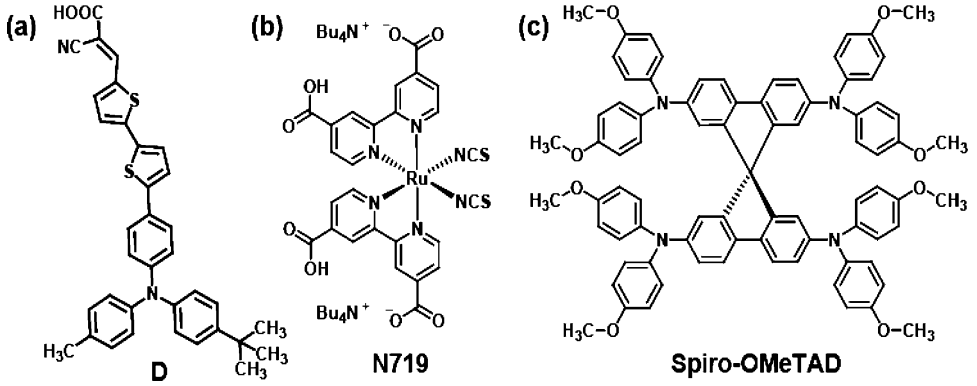

Figure 1. Chemical structures used in this study (a) **D**, (b) **N719**, and (c) spiro-OMeTAD.

understand the role of the interfacial properties and light harvesting characteristics on performance. We synthesized the organic dye 3-(5′-(4-(4-tert-butyl-phenyl-(4-fluoro-phenyl)-amino)-phenyl)-(2,2′)bithiophenyl-5-yl)-2-cyanoacrylic acid (**D**) from triphenylamine (TPA) and tested the dye in DSCs with liquid electrolyte or solid HTM systems to compare the properties of the organic dye with those of ruthenium complexes (**N719**).

Triphenylamines are strongly electron-donating in the context of organic dyes[29,30] or organic electronics.[31] A tertiary butyl end functional group was selected here to reduce intermolecular interactions among dyes and to minimize dye aggregation.[32] The other end group was a methyl, selected to tune the energy levels to those of the other components in the DSC. The photovoltaic performance, LHE, and interfacial properties of **D**-sensitized devices were compared with those of **N719**-sensitized devices. As expected, the photovoltaic behavior of the **D**-sensitized device based on a liquid junction differed significantly from the behavior of **N719**-sensitized and solid-state **D**-sensitized devices, for various TiO_2 electrode layer thicknesses. The UV–vis absorption and transmittance spectra were used to quantify the light harvesting ability. Electrochemical impedance spectroscopy (EIS),[33,34] intensity modulated photocurrent spectroscopy (IMPS), and intensity modulated photovoltage spectroscopy (IMVS) were used to examine the charge transfer/transport properties at the surface of the TiO_2 electrode.[35]

EXPERIMENTAL SECTION

Synthesis of Sensitizer. The synthesis of sensitizer 3-(5′-(4-(4-*tert*-butyl-phenyl-(4-fluoro-phenyl)-amino)-phenyl)-(2,2′)-bithiophenyl-5-yl)-2-cyanoacrylic acid (**D**) was done by modified scheme which is reported elsewhere.[30]

Characterization of Sensitizer. To investigate the electrochemical properties of the dyes, cyclic voltammetry measurements (CV) were carried out in a acetonitrile solution containing tetrabutyl ammonium tetrafluoroborate, TBA (BF_4) using a dye-coated TiO_2 film (2 μm) as a working, Ag/AgCl reference electrode and a Pt wire as a counter electrode with scan rate of 50 mV s^{-1}. Ferrocenium/ferrocene (Fc/Fc+) redox couple was used as an internal reference and potentials measured were converted to normal hydrogen electrode (NHE) by addition of +0.69 V. The UV–vis absorption and transmittance spectra of the dye solution in ethanol and dye-coated TiO_2 films (1.5–13 μm) were recorded on a Cary 5 spectrophotometer and emission spectra were recorded on a JASCO FP-6500.

Fabrication of Dye-Sensitized Solar Cells. Dye-sensitized solar cells were fabricated on a fluorine-doped SnO_2 glass substrates (15 Ω/sq, Pilkington) after cleaning the substrate with Helmanex solution, deionized water, ethanol, and acetone in sequence. The 20 nm of nanocrystalline TiO_2 (Solaronix, T20/SP series) deposited by doctor blade technique to give various thicknesses of 2–8 μm. For solid-state DSC fabrication, a 100 nm compact layer of TiO_2 was coated by aerosol spray pyrolysis at 450 °C using oxygen as carrier gas[36] prior to the deposition of nc-TiO_2. Resulting TiO_2 films were then sintered at 500 °C under an oxygen flow. After they were cooled, the TiO_2 films were immersed in 40 mM of $TiCl_4$ solution at 70 °C for 30 min and then rinsed with deionized water. The $TiCl_4$-treated TiO_2 films were sintered at 450 °C for 30 min and then cooled to 80 °C followed before immersing in dye solution (0.3 mM of dye dissolved in ethanol (**D**) or 1:1 v/v mixture of acetonitrile and *tert*-butanol (**N719**) for 12 h at room temperature. Liquid-DSCs were assembled with a platinized counter electrode and filled with an electrolyte containing 0.6 M butylmethyl immidazolium iodide (BMII), 0.03 M I_2, 0.1 M guanidinium thiocyanate (GuSCN), 0.5 M LiI, and 0.5 M 4-*tert*-butylpyridine (tBP) in a mixture of acetonitrile and valeronitrile (85:15 v/v). For sDSCs, the hole transporting material 2,2′,7,7′-tetrakis(*N*,*N*-di-p-methoxyphenylamine)-9,9′-spiro-bifluorene (spiro-OMeTAD) solution (0.17 M) with additives of tBP (0.11 M) and $Li[CF_3SO_2]_2N$ (21 mM) was spin-coated at 2000 rpm for 30 s on top of the TiO_2 film. Finally, a 100 nm gold layer was evaporated on the top of the spiro-OMeTAD under ultrahigh vacuum (UHV).

Photovoltaic Measurements. Photovoltaic measurements of the DSCs were carried out using a Keithley 2400 digital source meter controlled by a computer under illumination of simulated AM 1.5G solar light from an AM 1.5 solar simulator (Newport, M-91190A, with a 450 W xenon lamp). Power was regulated to the AM 1.5G solar standard by using a reference Si photodiode equipped with a color-matched filter (KG-3, Schott) to reduce the mismatch in the region of 350–750 nm between the simulated light and AM 1.5G to less than 4%. The impedance spectroscopes (EIS) of devices were measured using a computer-controlled potentiostat (SP-200, BioLogic) under dark conditions. The frequency range examined was 100 mHz – 1 MHz at room temperature, and the impedance spectra were recorded at potentials that varied from −0.40 to −0.75 V forward bias (−0.40 to −0.55 V for D-device-L, −0.50 to −0.60 V for N-device-L, and −0.55 to −0.75 V for solid-state DSCs) with a voltage amplitude set at 10 mV. The measured spectra were fit to appropriate equivalent circuits using the Z-fit software provided by BioLogic. The intensity-modulated measurements were carried out using a Zahner CIMPS response analyzer, which was used to derive a LED and to measure the optoelectronic transfer functions. The LED (λ = 480 nm) provided both the dc and ac components superimposed on the dc light was less than 10% in a range of 100 mHz to 1 kHz.

DFT Calculations. The molecular structures of dyes on $Ti_{44}O_{78}$ cluster are performed using the Dmol3 package based on density functional theory (DFT). In the Dmol3 electronic structure calculations, double numerical with d-polarization (DND) basis set are chosen. The density function is treated with the generalized gradient approximation (GGA) with the Perdew–Burke–Ernzerhof (PBE) exchange correlation potential. Dipole moments are calculated by using Hirshfeld population analysis method.

RESULTS AND DISCUSSION

Properties of the Sensitizers. The inset in Figure 2b shows the molar extinction coefficients (ε) of **D** and **N719**. The

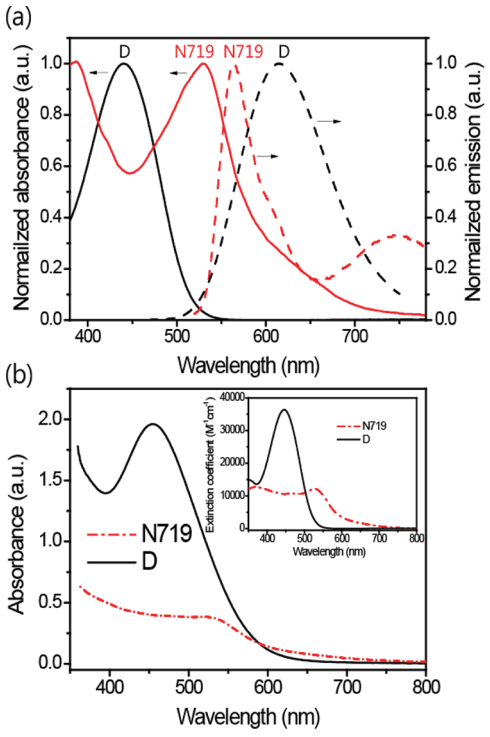

Figure 2. (a) Normalized absorbance (solid line) and emission (dashed line) spectra of **D** (black) and **N719** (red) in an ethanol solution. (b) Absorbance of **D**- (black solid line) and **N719** (red dotted line)-sensitized TiO_2 films. The inset shows the molar extinction coefficients (ε) of **D** and **N719** in ethanol solutions.

ε of **D** was 36 400 M^{-1} cm^{-1}, which was a factor of 3 greater than that of the ruthenium dye (Table 1). The band edge of **D** (520 nm) appeared at a shorter wavelength than that of **N719** (620 nm), indicating that the absorption window of **D** was relatively narrow. The absorption spectra of the dyes adsorbed onto 2 μm thick TiO_2 electrodes were similar to those of the solution spectra but red-shifted by 10 nm because of interactions between the anchoring groups and the surface titanium ions, aggregation of dyes, and scattering effects in the mesoporous TiO_2 (Figure 2b).[37] The absorbance of **D** in the film state was 5 times the absorbance of **N719**, indicating that more than 80% of **D** compared to **N719** were anchored onto the TiO_2 surface. The photoinduced current density (J_{SC}) of a device is influenced principally by the LHE, although other factors, such as charge separation (injection and dye regeneration) and charge collection, are also important. The LHE is governed by the amount of dye adsorbed onto a TiO_2 electrode, the extinction coefficient, and the absorption window of the dye. LHE, expressed as $1 - 10^{-\varepsilon\Gamma} = 1 - 10^{-A}$, where Γ is the dye loading per projected surface area of the film, and A is the absorption optical density of the sensitizer film, is frequently used to compare different dyes.[38] LHE estimates cannot generally be made based on the value of A measured from UV–vis absorption spectra because dye absorbance measurements can only be made on films with low levels of dye loading due to instrumental limitations. Therefore, we measured the film transmittance as a function of TiO_2 film thickness, as shown in Figure 3a. The percent transmittance of

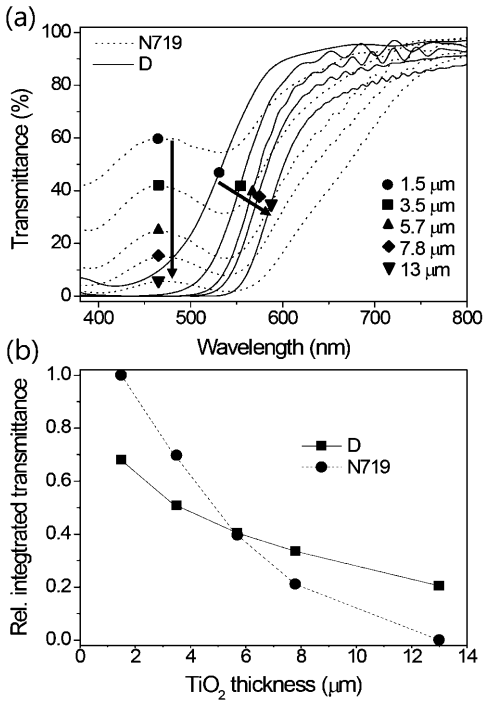

Figure 3. (a) % Transmittance of **D** (black solid line) and **N719** (red dotted line) for various TiO_2 film thicknesses, and (b) relative integrated transmittance of **D** (black square) and **N719** (red circle) as a function of TiO_2 film thickness.

N719 reached a maximum value at 470 nm over the range 400–550 nm, which corresponded to the lowest absorbance. The percent transmittance decreased with increasing thickness of TiO_2 film, indicating that the absorption of incident light by the dye increased with the TiO_2 film thickness.

A comparison of the percent transmittance of **N719** and **D** on 3.5 μm TiO_2 films highlighted the differences in the absorption spectra **D** and **N719**. The % transmittance of **N719** was ~30% at 530 nm. On the other hand, 3.5 μm **D**-sensitized TiO_2 completely absorbed the incident light at this wavelength, providing 0% transmittance due to the high loading and high ε of **D**. Figure 3b shows the relative integrated transmittances for various TiO_2 film thicknesses sensitized with **N719** or **D**. The integration values gradually decreased due to the high dye loading levels. In films thicker than 5.7 μm, **N719** yielded a lower integrated transmittance than **D**, mainly because of the

Table 1. Absorption/Emission Spectra and the Electrochemical Properties of D and N719

	Abs_{max} [nm] solution[a]	film	ε [$M^{-1}cm^{-1}$]	Em_{max} [nm][a]	$E_{(S+/S)}$ [V]	$E_{(0-0)}$ [V]	$E_{(S+/S^*)}$ [V]
D	445	456	36 400	622	1.10	2.35	−1.25
N719	530	540	13 000	564	0.8	1.6	−0.8

[a]The absorption and emission spectra in solution were measured using ethanol as a solvent.

dx.doi.org/10.1021/am300480j | ACS Appl. Mater. Interfaces 2012, 4, 3141–3147

broad absorption window of **N719**, particularly at long wavelengths.

The electrochemical properties of the organic dyes were measured using cyclic voltammeter (Figure 4a). The oxidation

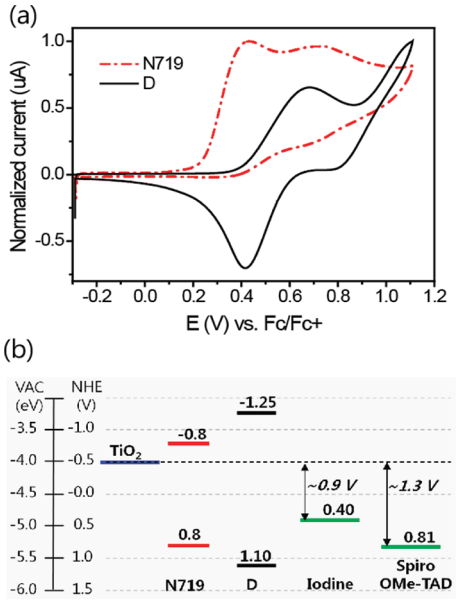

Figure 4. (a) Cyclic voltammograms of **N719**- and **D**-sensitized TiO_2 films. (b) Relative energy levels of the materials used in this study and expected theoretical V_{OC} for liquid electrolyte (I^-/I_3^-) or HTM (spiro-OMeTAD).

potential $E_{(S+/S)}$ of a **D**-sensitized thin TiO_2 film appeared at 1.10 V vs NHE (Table 1). The excited-state oxidation potential $E_{(S+/S^*)}$ was −1.25 V, obtained from the equation: $E_{(S+/S^*)} = E_{(S+/S)} - E_{(0-0)}$, where $E_{(0-0)}$ is determined from the intercept of the absorption and emission spectra (Figure 2a).

A model of the energy levels of all components was constructed based on the values obtained from individual experiments, as shown in Figure 4(b). The energy gap for electron extraction (ΔG_{ext}) from the lowest unoccupied molecular orbital (LUMO) of **D** to the conduction band was 0.75 V, which was much larger than that between the LUMO of **N719** and the conduction band. The energy gap for dye-regeneration (ΔG_{reg}) between the highest occupied molecular orbital (HOMO) of **D** and redox species, such as I^-/I_3^- or spiro-OMeTAD, was larger than that between the HOMO of **N719** and the redox species, suggesting the better performance would be achieved in devices employing **D**.

Photovoltaic Performances in Liquid-DSCs. The effects of the LHE on solar cell performance were examined in liquid-DSCs employing I^- and I_3^- redox couples at various film thicknesses without light scattering layers (Figure 5a). The parameters for these cells are summarized in Table 2. The J_{SC} of **N719**-sensitized liquid junction cells (denoted **N-device-L**) increased significantly from 4.22 mA/cm^2 to 13.2 mA/cm^2 with increasing device thickness, from 2 to 8 μm. The **D**-sensitized liquid junction devices (denoted as **D-device-L**) increased to a lesser degree from 6.43 mA/cm^2 to 7.28 mA/cm^2. In the 4 μm thick device, the J_{SC} of **D-device-L** was smaller than that of the **N-device-L**, even though the LHE of the **D**-sensitized film was higher than that of **N719**-sensitized film, as shown in Figure 2(b). This result indicates that photogenerated electrons were not efficiently transformed into current in the **D-device-L**.

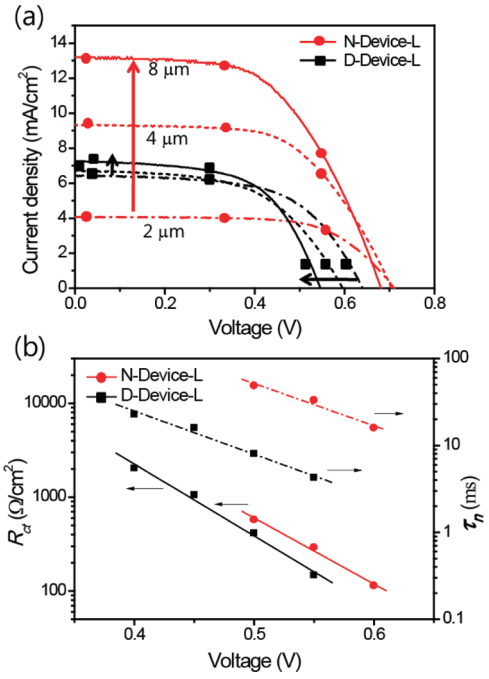

Figure 5. (a) $I-V$ characteristics of **D**-sensitized solar cells (**D-device-L**; black line) and **N719**-sensitized solar cells (**N-device-L**; red line) using a liquid electrolyte at various film thicknesses (2 μm, dash dotted; 4 μm, dotted; 8 μm, solid line). (b) R_{ct} (solid line) and τ_n (dash dotted line) for **D-device-L** (black square) and **N-device-L** (red circle) from the EIS measurements.

Table 2. Photovoltaic Performance of DSCs Incorporating D and N719 under 1 Sun Intensity of Light[a]

dye	film thickness [μm]	J_{SC} [mA/cm^2]	V_{OC} [V]	FF	η [%]
D	2	6.43	0.64	0.60	2.45
	4	6.70	0.60	0.55	2.21
	8	7.28	0.55	0.59	2.35
N719	2	4.22	0.70	0.63	1.87
	4	9.34	0.71	0.60	3.93
	8	13.2	0.68	0.56	5.03

[a]Active area of 0.25 cm^2 and AM 1.5G photon flux

V_{OC} is defined by the energy difference (0.9 V) between the quasi-Fermi level in the TiO_2 under illumination and the redox potential of the redox species. V_{OC} is sensitive to the presence of lithium ions and bases, such as tert-butylpyridine (tBP). The V_{OC} values measured in both devices were much lower than the theoretical value and, unexpectedly, the V_{OC} of **D-device-L** was in a range 0.55−0.64 V, which was smaller than that of **N-device-L** (0.68−0.71 V) under identical conditions. To rationalize this result the nature of the dyes, such as the dipole moment, could be considered as it can alter the conduction band of the TiO_2 electrode, resulting in a lower V_{OC}. However, the dipole moments of TPA-based organic dyes are generally exhibited negative value and thereby induce high electron density toward the surface of TiO_2,[28] suggesting that V_{OC} in **D-device-L** should be higher, which is opposite the result observed here. Indeed, the calculated dipole moment of **D** along with the z axis corresponds to the surface normal of TiO_2 was 1.45 debye, while that of N719 has been known to be lie between −23.1 to −29.0 debye, depending on the adsorption geometry.[39] Therefore, the differences in the dipole moments

dx.doi.org/10.1021/am300480j | ACS Appl. Mater. Interfaces 2012, 4, 3141−3147

of **D** and **N719** could not explain the difference of V_{OC} values for the **D-device-L** and for **N-device-L**.

As Nazeeruddin et al. proposed,[40] V_{OC} is strongly affected by recombination between photoinduced electrons and redox species, as described by the equation: $V_{OC} = (kT/e)\ln(I_{inj}/n_{cb}k_{et}[I_3^-])$, where I_{inj} is the charge flux from sensitized injection, n_{cb} is the surface electron concentration at the TiO_2 surface, and k_{et} is the rate constant for I_3^- reduction. Therefore, the lower V_{OC}s for **D-device-L** than those of **N-device-L** may contribute to fast recombination reaction of photoinduced electrons with I_3^- in liquid electrolyte. Indeed, EIS revealed that the charge recombination resistance (R_{ct}) and electron lifetime (τ_n) for **D-device-L** on the thick (8 μm) or thin (2 μm) TiO_2 electrodes were smaller than those for **N-device-L** (Figure 5(b), 6(a) and Table 3). Such less efficient passivation effect of

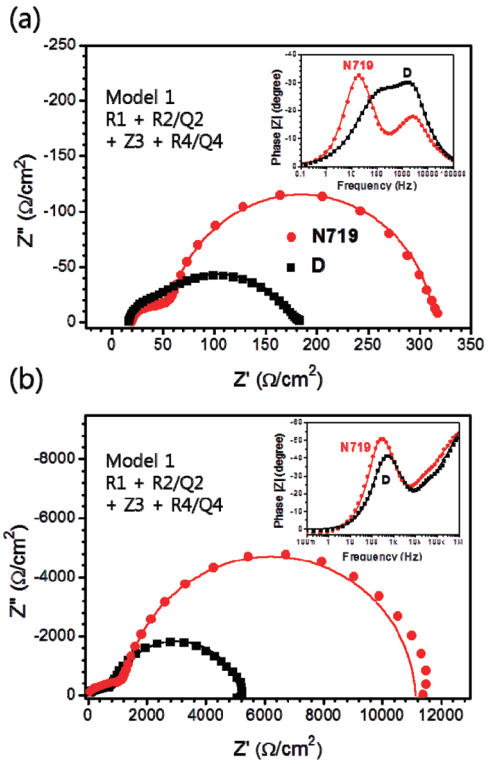

Figure 6. Nyquist plots: (a) Liquid state devices, **N-Device-L** (red circle) and **D-Device-L** (black square). (b) Solid state devices, **N-Device-S** (red circle) and **D-Device-S** (black square). Measurements were obtained using EIS at −0.55 V (liquid state devices) and −0.75 V (solid state devices) forward biases. The solid lines indicate fits to the data using an equivalent circuit (model1). The insets show bode phase plots for the devices. The equivalent circuit model to fit the experimental data is provided in the figure. In the model, R1, R2/C2, Z3, and R4/C4 represent series resistance, impedance at TiO_2/dye/electrolyte interface, Warburg impedance in the electrolyte, and impedance at counter electrode/electolyte interface, respectively.

D-sensitized TiO_2, especially, limits the enhancement of power conversion efficiency at thicker TiO_2 films. The estimated electron diffusion length (L_D) in 2 μm thick **D-device-L** (3.9 μm), calculated from the diffusion coefficient (D_n) and τ_n by the equation $L_D = (D_n\tau_n)^{1/2}$, which were measured using IMPS and IMVS,[41] respectively, were shorter than that of **N-device-L** (7.5 μm). Although the loading of **D** on the TiO_2 electrode surface was greater than the loading of **N719**, the passivation effects of **D** were not effective, probably due to the smaller molecular size of **D**. In turn, the values of J_{SC} in **D-device-L** increased slightly from 6.43 mA/cm^2 (2 μm) to 7.28 mA/cm^2 (8 μm), whereas V_{OC} decreased from 0.64 V (2 μm) to 0.55 V (8 μm), with increasing thickness of the TiO_2 electrodes, in contrast with the trends observed for **N719**.

Photovoltaic Performance of the Solid-DSCs. We investigated the passivation effect observed in liquid-DSCs by fabricating solid-DSCs employing spiro-OMeTAD as an organic HTM. TiO_2 electrodes 2 μm thick were chosen for the fabrication of solid-DSCs to obtain good pore filling in the TiO_2 electrodes. Figure 7(a) shows the $I-V$ characteristics of solid-DSCs sensitized with **D** (**D-device-S**) and **N719** (**N-device-S**), and their photovoltaic parameters are summarized in Table 4.[42] Under identical condition[43] with 0.17 M spiro-OMeTAD, 21 mM Li-TFSI, and 110 mM t-BP, the V_{OC} of **D-device-S** was 0.98 V, which was 0.23 V higher than that of **N-device-S** (0.75 V). This is opposite result with that observed in liquid-DSC, suggesting the interfacial properties are quite different when the dye-coated TiO_2 contact with liquid electrolyte or solid HTM. From the energetic point of view, the energy difference between HOMO level of spiro-OMeTAD and the HOMO level of N719 is too small to provide enough driving forces for the regeneration of oxidized **N719**, unlike the **D**. Furthermore, the charge transfer and charge transport phenomena of solid-state devices sensitized with **N719** and **D** were significantly different from the result of liquid-DSCs. The EIS result clearly shows the difference, that is, the R_{ct} of solid-DSC is significant higher (4400 and 10 400 Ω/cm^2 for **D-device-S** and **N-device-S**, respectively) than the corresponding liquid-DSCs, while the τ_ns for the **D** and **N719** solid-DSCs were shorter than in the corresponding liquid-DSSs, as seen Table 3 and Figure 7b.

Such difference may attribute to the fact that the dyes form a monolayer between the surface of TiO_2 electrodes and the solid HTM, partially insulating the electrode from the HTM, and the physical contact could be quite different compared to that in liquid-DSCs, in which redox species and dyes anchored to the surface of TiO_2 electrodes were dissolved in liquid electrolyte, thus redox species could directly reach the surfaces of the TiO_2. As a result, the insulation by dye monolayer in solid-state could induce several different phenomena. First, the estimated L_D of solid-DSCs were almost same for **D-device-S** (3.0 μm) and **N-device-S** (2.9 μm) although the τ_n of **D-device-S** was shorter than that of **N-device-S**, due to the higher D_n of **D-device-S**, indicating the device thickness is not a limiting factor for the two dyes. In addition, the real energy level of the materials at the heterojunction would be quite different from the measured value as S. Haque and T. Park proposed,[16] i.e. the contact properties of dye-coated TiO_2 and liquid electrolyte or solid HTM and the resulting energy level of the conduction band of the TiO_2 are different as shown in Figure 8. Thus, the significant higher V_{OC} of **D-device-S** when compare to **D-device-L**, unlike the result from **N719-device**, is probably due to higher surface dipole (χ_{dip}) of **D**-sensitized TiO_2 which induce negative shift of CB of TiO_2 electrode or positive shift of HOMO level of spiro-OMeTAD when it contacts with **D** rather than **N719**.

The changes in V_{OC} due to the interfacial properties at the TiO_2 electrode surface were examined. V_{OC} is sensitive to the recombination rate and TiO_2 surface state energies, which can shift, negatively or positively, depending on the surface dipole potential (χ_{dip}) induced by additives, such as tBP. In general, tBP negatively shifted the CB of TiO_2 but decreased the driving

dx.doi.org/10.1021/am300480j | ACS Appl. Mater. Interfaces 2012, 4, 3141−3147

Table 3. Recombination Resistance (R_{ct}), Electron Lifetime (τ_n), Diffusion Coefficient (D_n), and Electron Diffusion Length (L_D) of DSCs Using Liquid Electrolytes and Solid HTM

system	dye	thickness (μm)	R_{ct} (Ω/cm^2)	τ_n[a] (ms)	D_n[b] ($\times 10^{-5}$ cm^2/s)	L_D[b] (μm)
liquid	**D**	2.0	865	10.8	0.56	3.9
electrolyte		8.0	150	8.6		
	N719	2.0	1,540	24.4	0.56	7.5
		8.0	290	15.3		
solid	**D**	2.0	4,400	0.8	1.66	3.0
HTM	**N719**	2.0	10,400	1.9	1.17	2.9

[a]Obtained from EIS results. [b]Obtained from IMPS/IMVS results. The L_D was calculated from the equation $L_D = (D_n\tau_n)^{1/2}$, where the τ_n value also obtained from IMVS measurement.

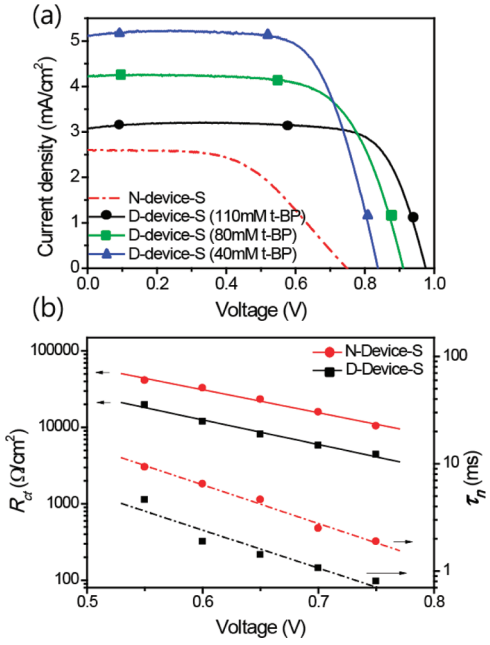

Figure 7. (a) $I-V$ characteristics of **D**-sensitized solar cells (**D-device-S**; black line) at various concentrations of the tBP additive (110 mM, black circle; 80 mM tBP, green square; 40 mM tBP, blue triangle) and **N719**-sensitized solar cells (**N-device-S**; red line) using spiro-OMeTAD as the HTM. (b) R_{ct} (solid line) and τ_n (dash dotted line) for **D-device-S** (black square) and **N-device-S** (red circle) calculated from EIS measurements.

Table 4. Photovoltaic Performance of ssDSCs Incorporating D and N719 under 1 Sun Intensity of Light[a]

dye	concentration of tBP [mM]	J_{SC} [mA/cm^2]	V_{OC} [V]	FF	η [%]
D	40	5.1	0.84	0.70	3.00
	80	4.0	0.95	0.72	2.70
	110	3.1	0.98	0.77	2.30
N719	110	2.6	0.75	0.53	1.03

[a]Active area of 0.16 cm^2 and AM 1.5G photon flux.

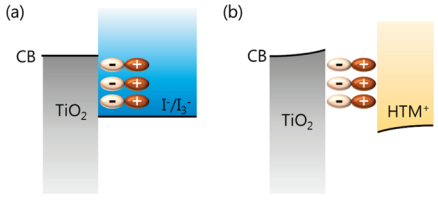

Figure 8. Relative energy levels in DSCs in (a) liquid state and (b) solid state at the heterojunction of TiO_2/dye/electrolyte(HTM).

force for electron injection from an excited dye to the CB of TiO_2. As shown in Figure 7a, V_{OC} of **D-device-S** gradually decreased, but J_{SC} increased significantly as the concentration of tBP decreased, indicating a better electron injection efficiency at low tBP due to a positive shift in the conduction band of TiO_2. This, in turn, decreased V_{OC}. The combined effects enhanced the power conversion efficiency from 2.3% to 3.0%, resulting in a factor of 3 higher efficiency than in the **N-device-S** under optimized conditions.

CONCLUSIONS

Triphenylamine-based organic dyes (**D**) were synthesized and tested in DSCs with comparison to the ruthenium complex **N719**. Despite the unique optical properties of **D**, such as a high extinction coefficient and high achievable loading levels, its low absorption window and fast recombination rate at the surface limited the utility of **D** on thick TiO_2 electrodes in liquid-DSCs. However, in solid-DSCs, the unique optical properties of **D** increased the LHE of **D**-sensitized devices relative to **N719**-sensitized devices. This was due to differences in the physical contact between the **D**- or **N719**-sensitized TiO_2 surfaces and the solid HTM or liquid electrolyte. **D** effectively acted as an insulating monolayer in contact with HTM, which dramatically increased R_{ct} and resulted in an increase in V_{OC}. The electron transport-limited **N-device-S**, however, showed a lower or comparable electron diffusion length and did not provide better performances than the **D-device-S**. These results indicate the importance of the interfacial properties and suggest strategies for further enhancing organic DSCs via molecular engineering of the interface.

AUTHOR INFORMATION

Corresponding Author

*E-mail: taihopark@postech.ac.kr. Fax: (+82) 54 2798298. Tel: (+82) 542795295.

Notes

The authors declare no competing financial interest.

ACKNOWLEDGMENTS

This work was supported by a grant (M2009010025) from the Fundamental R&D Program for Core Technology of Materials funded by the MKE, the Midcareer Researcher Program (No. 2010-0000406), and the Future-based Technology Development Program (Nano Fields, No. 2010-0019119) through NRF, funded by the MEST, and by the second stage of a BK21 (Brain Korea 21). Partial support for this work was provided by POSCO.

REFERENCES

(1) O'Regan, B.; Grätzel, M. *Nature* **1991**, *353*, 737.
(2) Lim, J.; Kwon, Y. S.; Park, T. *Chem. Commun.* **2011**, *47*, 4147.
(3) Lim, J.; Kwon, Y. S.; Park, S.-H.; Song, I. Y.; Choi, J.; Park, T. *Langmuir* **2011**, *27*, 14647.
(4) Park, S. −H.; Lim, J.; Song, I. Y.; Atmakuri, N.; Song, S.; Kwon, Y. S.; Choi, J. M.; Park, T. *Adv. Energy Mater.* **2012**, *2*, 219.
(5) Hamann, T. W.; Jensen, R. A.; Martinson, A. B. F.; Ryswyk, H. V.; Hupp, J. T. *Energy Environ. Sci.* **2008**, *1*, 66.
(6) Hagfeldt, A.; Boschloo, G.; Sun, L.; Kloo, L.; Pettersson, H. *Chem. Rev.* **2010**, *110*, 6595.
(7) Goncalves, L. M.; Bermudez, V. Z.; Ribeiro, H. A.; Mendes, A. M. *Energy Environ. Sci.* **2008**, *1*, 655.
(8) Nazeeruddin, M. K.; De Angelis, F.; Fantacci, S.; Selloni, A.; Viscardi, G.; Liska, P.; Ito, S.; Takeru, B.; Grätzel, M. *J. Am. Chem. Soc.* **2005**, *127*, 16835.
(9) Chiba, Y.; Islam, A.; Watanabe, Y.; Komiya, R.; Koide, N.; Han, L. *Jpn. J. Appl. Phys.* **2006**, *45*, L638.
(10) Mishra, A.; Fischer, M. K. R.; Bäuerle, P. *Angew. Chem., Int. Ed.* **2009**, *48*, 2474.
(11) Tian, H.; Yang, X.; Chen, R.; Hagfeldt, A.; Sun, L. *Energy Environ. Sci.* **2009**, *2*, 674.
(12) Li, C.; Yum, J.-H.; Moon, S.-J.; Herrmann, A.; Eickemeyer, F.; Pschirer, N. G.; Erk, P.; Schöneboom, J.; Müllen, K.; Grätzel, M.; Nazeeruddin, M. K. *ChemSusChem* **2008**, *1*, 615.
(13) Edvinsson, T.; Li, C.; Pschirer, N.; Schöneboom, J.; Eickemeyer, F.; Sens, R.; Boschloo, G.; Herrmann, A.; Müllen, K.; Hagfeldt, A. *J.Phys. Chem. C* **2007**, *111*, 15137.
(14) Hara, K.; Sayama, K.; Ohga, Y.; Shinpo, A.; Suga, S.; Arakawa, H. *Chem. Commun.* **2001**, 569.
(15) Wang, Z. S.; Cui, Y.; Dan-oh, Y.; Kasada, C.; Shinpo, A.; Hara, K. *J. Phys. Chem. C* **2007**, *111*, 7224.
(16) Tokuhisa, H.; Hammond, P. T. *Adv. Funct. Mater.* **2003**, *13*, 831.
(17) Sayama, K.; Tsukagoshi, S.; Mori, T.; Hara, K.; Ohga, Y.; Shinpou, A.; Abe, Y.; Suga, S.; Arakawa, H. *Sol. Energy Mater. Sol.Cells* **2003**, *80*, 47.
(18) Ito, S.; Zakeeruddin, S. M.; Humphry-Baker, R.; Liska, P.; Charvet, R.; Comte, P.; Nazeeruddin, M. K.; Péchy, P.; Takata, M.; Miura, H.; Uchida, S.; Grätzel, M. *Adv. Mater.* **2006**, *18*, 1202.
(19) Horiuchi, T.; Miura, H.; Sumioka, K.; Uchida, S. *J. Am. Chem. Soc.* **2004**, *126*, 12218.
(20) (a) Kwon, Y. S.; Song, I. Y.; Lim, J.; Park, S.-H.; Siva, A.; Park, Y.-C.; Jang, H. M.; Park, T. *RSC Adv.* **2012**, *2*, 3467. (b) Song, I. Y.; Park, S.-H.; Lim, J.; Kwon, Y. S.; Park, T. *Chem. Commun.* **2011**, *47*, 10395.
(21) Park, T.; Haque, S. A.; Potter, R. J.; Holmes, A. B.; Durrant, J. R. *Chem. Commun.* **2003**, *9*, 2878.
(22) Hague, S. A.; Park, T.; Xu, C.; Koops, S.; Schulte, N.; Potter, R. J.; Holmes, A. B.; Durrant, J. R. *Adv. Funct. Mater.* **2004**, *14*, 435.
(23) Snaith, H. J.; Petrozza, A.; Ito, S.; Miura, H.; Grätzel, M. *Adv. Funct. Mater.* **2009**, *19*, 1810.
(24) Liu, X.; Zhang, W.; Uchida, S.; Cai, L.; Liu., B.; Ramakrishna, S. *Adv. Mater.* **2010**, *22*, E150.
(25) Cai., N.; Moon, S.-J.; Cevey-Ha, L.; Moehl, T.; Humphry-Baker, R.; Wang, P.; Zakeeruddin, S. M.; Grätzel, M. *Nano Lett.* **2011**, *11*, 1452.
(26) Haque, S. A.; Park, T.; Holmes, A. B.; Durrant, J. R. *ChemPhysChem* **2003**, *4*, 89.
(27) Haque, S. A.; Palomares, E.; Cho, B. M.; Green, A. N. M.; Hirata, N.; Klug, D. R.; Durrant, J. R. *J. Am. Chem. Soc.* **2005**, *127*, 3456.
(28) Miyashita, M.; Sunahara, K.; Nishikawa, T.; Uemura, Y.; Koumura, N.; Hara, K.; Mori, A.; Abe, T.; Suzuki, E.; Mori, S. *J. Am. Chem. Soc.* **2008**, *130*, 17874.
(29) (a) Kwon, Y. S.; Lim, J.; Song, I.; Song, I. Y.; Shin, W. S.; Moon, S.-J.; Park, T. *J. Mater. Chem.* **2012**, *22*, 8641. (b) Hwang, S.; Lee, J. H.; Park, C.; Lee, H.; Kim., C.; Park, C.; Lee, M.-H.; Lee, W.; Park, J.; Kim, K.; Park, N. −G.; Kim, C. *Chem. Commun.* **2007**, 4887.
(30) Yum., J.-H.; Hagberg, D. P.; Moon, S.-J.; Karlsson, K. M.; Marinado, T.; Sun, L.; Hagfeldt, A.; Nazeeruddin, M. K.; Grätzel, M. *Angew. Chem., Int. Ed.* **2009**, *48*, 1576.
(31) Huang, Q.; Evmenenko, G. A.; Dutta, P.; Lee., P.; Armstrong, N. R.; Marks, T. J. *J. Am. Chem. Soc.* **2005**, *127*, 10227.
(32) Lu, H.-P.; Tsai, C.-Y.; Yen, W.-N.; Hsieh, C.-P.; Lee, C.-W.; Yeh, C.-Y.; Diau, E. W.-G. *J. Phys. Chem. C* **2009**, *113*, 20990.
(33) Fabregat-Santiago, F.; Bisquert, J.; Cevey, L.; Chen, P.; Wang, M.; Zakeeruddin, S. M.; Grätzel, M. *J. Am. Chem. Soc.* **2009**, *131*, 558.
(34) Li, X.; Lin, H.; Li, J.; Li, X.; Cui, B.; Zhang, L. *J. Phys. Chem. C* **2008**, *112*, 13744.
(35) Krüger, J.; Plass, R.; Grätzel, M.; Cameron, P. J.; Peter, L. M. *J. Phys. Chem. B* **2003**, *107*, 7536.
(36) Kavan, L.; Grätzel, M. *Electrochim. Acta* **1995**, *40*, 643.
(37) Moon, S.-J.; Yum, J.-H.; Humphry-Baker, R.; Karlsson, K. M.; Hagberg, D. P.; Marinado, T.; Hagfeldt, A.; Sun, L.; Grätzel, M.; Nazeeruddin, M. K. *J. Phys. Chem. C* **2009**, *113*, 16816.
(38) Chen, P.; Yum, J.-H.; De Angelis, F.; Mosconi, E.; Fantacci, S.; Moon, S.-J.; Humphry-Baker, R.; Ko., J.; Nazeeruddin, M. K.; Grätzel, M. *Nano Lett.* **2009**, *9*, 2487.
(39) De Angelis, F.; Fantacci, S.; Selloni, A.; Grätzel, M.; Nazeeruddin, M. K. *Nano Lett.* **2007**, *7*, 3189.
(40) Nazeeruddin, M. K.; Rodicio, A. K. I.; Humphry-Baker, R.; Müller, E.; Liska, P.; Vlachopoulos, N.; Grätzel, M. *J. Am. Chem. Soc.* **1993**, *115*, 6382.
(41) Wang, H.; Peter, L. M. *J. Phys. Chem. C* **2009**, *113*, 18125.
(42) Relatively low η for control device may be due to the use of N719, which is not best Ru dyes for solid-DSCs instead of most frequently used Z907 dye and also due to low purity of homemade spiro-OMeTAD.
(43) Wang, M.; Grätzel, C.; Moon, S.-J.; Humphry-Baker, R.; Rossier-Iten, N.; Zakeeruddin, S. M.; Grätzel, M. *Adv. Funct. Mater.* **2009**, *19*, 2163.